$3^2S_{1/2}$-$3^2D_{5/2}$ interval in atomic hydrogen. II. Experiment and results

B. O. Clark,* D. A. Van Baak, S. R. Lundeen, and F. M. Pipkin

Lyman Laboratory of Physics, Harvard University, Cambridge, Massachusetts 02138

(Received 8 August 1978)

This paper reports a double-quantum radiofrequency measurement of the $3^2S_{1/2}$-$3^2D_{5/2}$ fine-structure interval in hydrogen. The measurement was carried out in zero magnetic field with a fast hydrogen beam. The measured value for the $3^2S_{1/2}$-$3^2D_{5/2}$ interval is 4013.204(78) MHz. This is in good agreement with the theoretical value.

I. INTRODUCTION

As pointed out in the previous paper,[1] the $3\,^2S_{1/2}$-$3\,^2D_{5/2}$ two-photon transition in hydrogen has a smaller natural linewidth than either the 3S-3P or 3D-3P fine-structure transitions. This makes this two-photon transition attractive as a source for a precision measurement of the hydrogen fine structure. Because of the 158-nsec lifetime of the $3\,^2S_{1/2}$ state and its high susceptibility to environmental perturbations, it is difficult to measure the fine structure in the $n=3$ state of hydrogen using either a thermal beam[2] or the bottle method.[3] The development of the fast-beam radio-frequency spectroscopy method has made it possible to overcome these problems and made it feasible to make high-precision measurements of the fine structure in the higher excited states of hydrogen.[4]

This paper reports a precision measurement of the $3\,^2S_{1/2}$-$3\,^2D_{5/2}$ two-photon electric dipole transition in hydrogen using fast-beam radio-frequency spectroscopy. The line-shape theory developed in the previous paper[1] is used to analyze the data. This paper treats in succession the fast-atomic-beam apparatus, the radio-frequency spectroscopy system, the data acquisition, the data reduction and results, and the conclusions.

II. APPARATUS

A schematic diagram of the fast-beam apparatus is shown in Fig. 1, together with an energy-level diagram which symbolically illustrates the relevant atomic processes occurring in each region of the apparatus. The fast beam of hydrogen atoms is produced by fragmentation and charge-exchange collisions between an incident beam of H_3^+ molecular ions and molecules of nitrogen "confined" to a target cell. The cell is simply a long hole (2.5-mm diam. by 125-mm length) drilled through a block of aluminum, with gas leaked into the center of the channel. This target design allows a large pressure gradient to exist over the length of the target cell, and defines the atomic beam geometry. The small aperture of the target cell and a bending magnet in the ion accelerator also serve to define the energy of the beam. With the input gas pressure near 40 mTorr, the beam neutralization fraction was roughly 50%. The motivation for using the molecular ion H_3^+ as the incident ion was to achieve as slow an atomic speed as possible given the lower energy limit ($\simeq 30$ keV) of the accelerator; the use of a slower beam results in narrower resonances. Remarkably, H^+, H_2^+, and H_3^+ were found to produce atoms in the 3S state with similar efficiency in a nitrogen target.

Hydrogen atoms emerge from the target cell in various substates of the $n=3$ manifold, as indicated by the cross-hatched areas in the level diagram of Fig. 1. However, only the $3\,^2S_{1/2}$ state has a sufficiently long lifetime (158 nsec) to allow atoms initially in this state to survive the length of the apparatus. The short lifetimes of the 3P states (5.4 nsec) and the 3D states (15.6 nsec) ensure that no appreciable numbers of atoms in these states will reach the spectroscopy region. If one neglects cascades from higher-n states, the number of Balmer α photons detected downstream by the photomultiplier tube and interference filter will be proportional to the number of atoms present in 3S states.
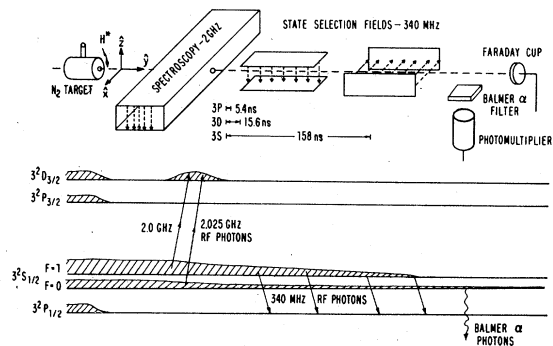

FIG. 1. Conceptual design of the experiment, showing in cross hatching the behavior of the populations of $n=3$ sublevels.
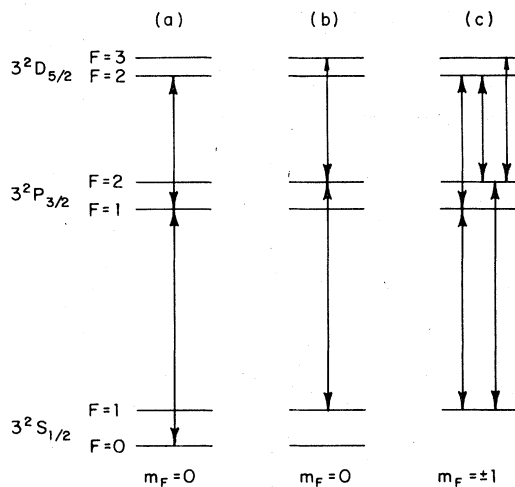
FIG. 2. Level diagram (not to scale) showing allowed $\Delta m_F = 0$ double-quantum transitions between $3\,^2S_{1/2}$ and $3\,^2D_{5/2}$ states, originating in (a) the $F = 0$, $m_F = 0$ state; (b) the $F = 1$, $m_F = 0$ state, and (c) the $F = 1$, $m_F = \pm 1$ states.

The spectroscopy region consists of a rectangular waveguide (of dimensions $a = 130$ mm by $b = 65$ mm) whose propagation axis is perpendicular to the atomic beam axis. Two small holes (8-mm diam.) are placed in the center of the narrow side walls of the waveguide to allow the atomic beam to enter and exit. In the TE_{10} mode, the microwave electric field in the waveguide is linearly polarized in the vertical (z) direction and will drive only the $\Delta m_F = 0$ transitions in the $n = 3$ manifold, where the axis of quantization has been chosen to coincide with the z polarization of the electric field. If the applied microwave frequency is resonant with any of the $3\,^2S_{1/2}$-$3\,^2D_{5/2}$ double-quantum transitions, some of the atoms in the $3\,^2S_{1/2}$ state will be transferred to the $3\,^2D_{5/2}$ state, and subsequently lost from the $n = 3$ manifold because of the rapid radiative decay of the $3\,^2D_{5/2}$ states. Thus, the Balmer α count rate downstream reflects the resonant double-quantum depopulation of the $3\,^2S_{1/2}$ states.

Owing to hyperfine structure, there are, as shown in Fig. 2, three allowed double-quantum transitions between the $3\,^2S_{1/2}$ and the $3\,^2D_{5/2}$ states. Two of these resonances occur between the $3\,^2S_{1/2}(F = 1)$ substates and the $3\,^2D_{5/2}(F = 2, 3)$ substates (and are hereafter referred to as F_1 resonances). These two resonances occur near 2000 MHz and are strongly overlapping. The third resonance occurs near 2025 MHz, between the $3\,^2S_{1/2}(F = 0)$ and the $3\,^2D_{5/2}(F = 2)$ substates (and is hereafter called the F_0 resonance). This latter resonance is suitable for a precision measurement, provided some way is found to desensitize the apparatus to the F_1 resonances. This is accomplished in the state selection fields which pre-

cede the photodetection region. An oscillating electric field at 330 MHz preferentially mixes the $3\,^2S_{1/2}(F = 1)$ states with the $3\,^2P_{1/2}(F = 0, 1)$ states, but leaves the $3\,^2S_{1/2}(F = 0)$ state relatively unperturbed. The lifetime of the unwanted atoms initially in the $3\,^2S_{1/2}(F = 1)$ states is thus greatly reduced, and it is possible to eliminate over 90% of the F_1 resonances without seriously affecting the F_0 resonance. The state selection fields are in two different polarizations so that both $\Delta m_F = 0$ and $\Delta m_F = \pm 1$ transitions between the $3\,^2S_{1/2}(F = 1)$ and the $3\,^2P_{1/2}(F = 0, 1)$ states are induced.

Figure 3 gives a block diagram of the electronic and microwave systems. The state selection fields are continuously driven by a microwave oscillator and tuned amplifier, with an rf diode used to monitor the microwave power. The microwave spectroscopy system will be discussed in some detail shortly. The microwave field in the waveguide is switched on and off at a 62.5-Hz rate, so that the survival rate of the $3\,^2S_{1/2}(F = 0)$ states can be measured with and without the microwave field. The output of the photomultiplier tube is synchronously gated into either counter B (rf off) or C (rf on). The atomic beam is stopped in a Faraday cup, which collects the charge of the unneutralized part of the original ion beam. The current output of the Faraday cup is converted into a pulse rate which is also gated into two counters, D (rf off) and E (rf on). The effects of short term variations in incident ion beam intensity on the experimental signals can be largely removed by dividing the photon count rate by the ion current. The experimental signal is thus defined as

$$S = \frac{B/D - C/E}{B/D} \times 100\%$$

which represents the fractional decrease of photon count rate upon application of the spectroscopy power, corrected to unit incident ion beam intensity. A typical linescan of the resonance is obtained by measuring the signal at many frequencies with the microwave field strength held constant.

The entire spectroscopy region is contained within three mutually orthogonal pairs of large magnetic field-compensation coils, operated so as to cancel all components of the earth's, and other stray, magnetic fields, to a typical tolerance of 20 mG ($= 2\mu T$).

III. MICROWAVE SPECTROSCOPY SYSTEM

To exploit the advantages of high-Q multiple-quantum transitions, it is essential that the microwave spectroscopy system be carefully designed and thoroughly understood. Unlike single-quantum transitions, the center frequency of a multiple-
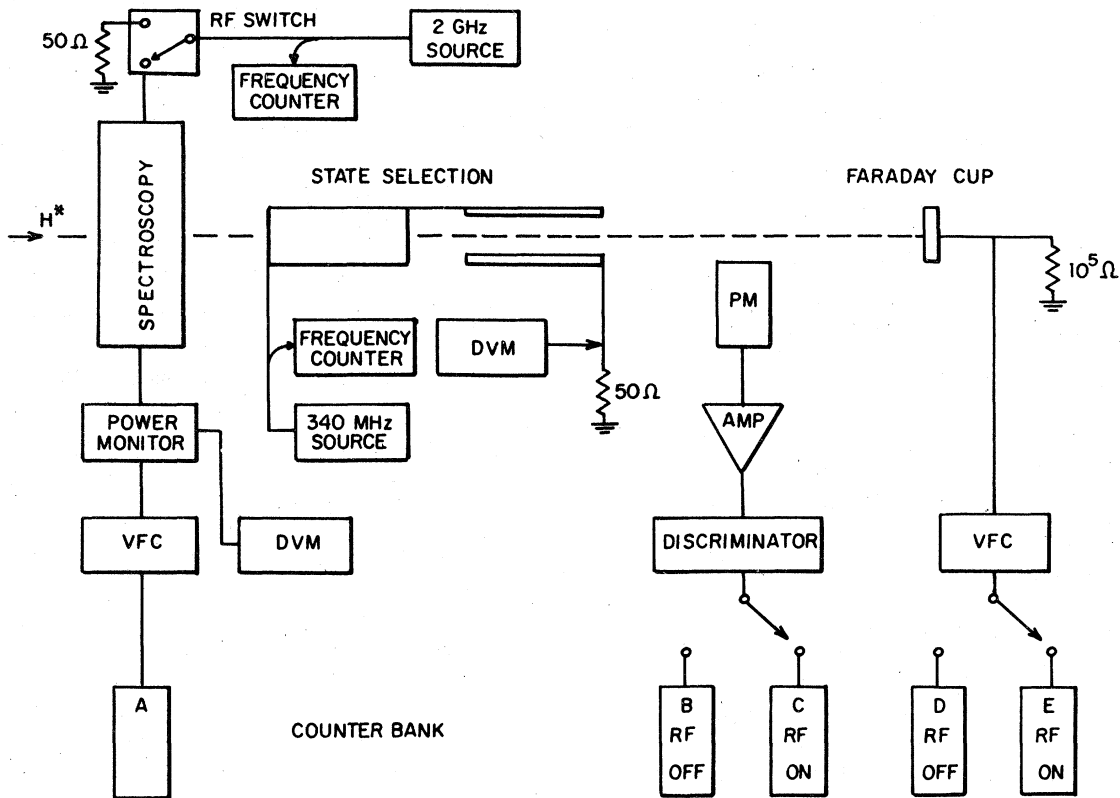
FIG. 3. Electronics and data collection system for the experiment.

quantum resonance depends upon the microwave power level and thus also upon the shape of the envelope of the microwave field. This necessitates a very good knowledge of the absolute, as well as the relative, power level, and an understanding of the shape of the microwave field. This is in addition to the stringent requirement of maintaining a constant electric field strength independent of microwave frequency. For an N-photon transition of width W, the unsaturated signal is proportional to E^{2N}, and thus a fractional error of $\Delta E/E$ over the linewidth will shift the apparent location of the line center by

$$\Delta \nu \propto NW(\Delta E/E) .$$

Figure 4 shows the microwave spectroscopy system in detail. Because we use rectangular waveguide operating in the TE_{10} mode with small beam access holes in the side walls, we can calculate with confidence the field shape within the waveguide and in the vicinity of the holes. The power transmitted through the waveguide at frequency ν is related to the peak electric field E by

$$P = (ab/4\mu_0 c)E^2(1 - \nu_c^2/\nu^2)^{1/2} ,$$

where $\nu_c = c/2a$ and c is the speed of light. Since the impedance of the waveguide is slowly changing

with frequency, it is important that E and not the power be kept constant. The placement of the holes in the narrow side wall as opposed to the broad wall is required to prevent, in the region of the holes, the existence of electric fields polarized normal to the electric field of the TE_{10} mode. Any such field components will induce $\Delta m_F = \pm 1$ transitions and will thus couple the F_0 and F_1 transitions.

Ideally, the waveguide acts as a perfect reflectionless transmission line and all the microwave power injected is absorbed in the attenuators and rf diode. Any reflected microwaves will produce a standing-wave pattern in the spectroscopy region, with the result that power maxima and minima will sweep past the atomic beam as the frequency is varied. Consequently, only microwave components with low reflection coefficients were used and reflection coefficients of all components were measured on a slotted line. The reflection coefficient of the waveguide to coaxial transformer at the output end is particularly important. This reflection coefficient was measured every 2.5 MHz over the band 2015 to 2040 MHz, and found to have a magnitude 0.028 ± 0.001, independent of frequency within the quoted error (which includes the residual errors of the slotted line system). The phase of
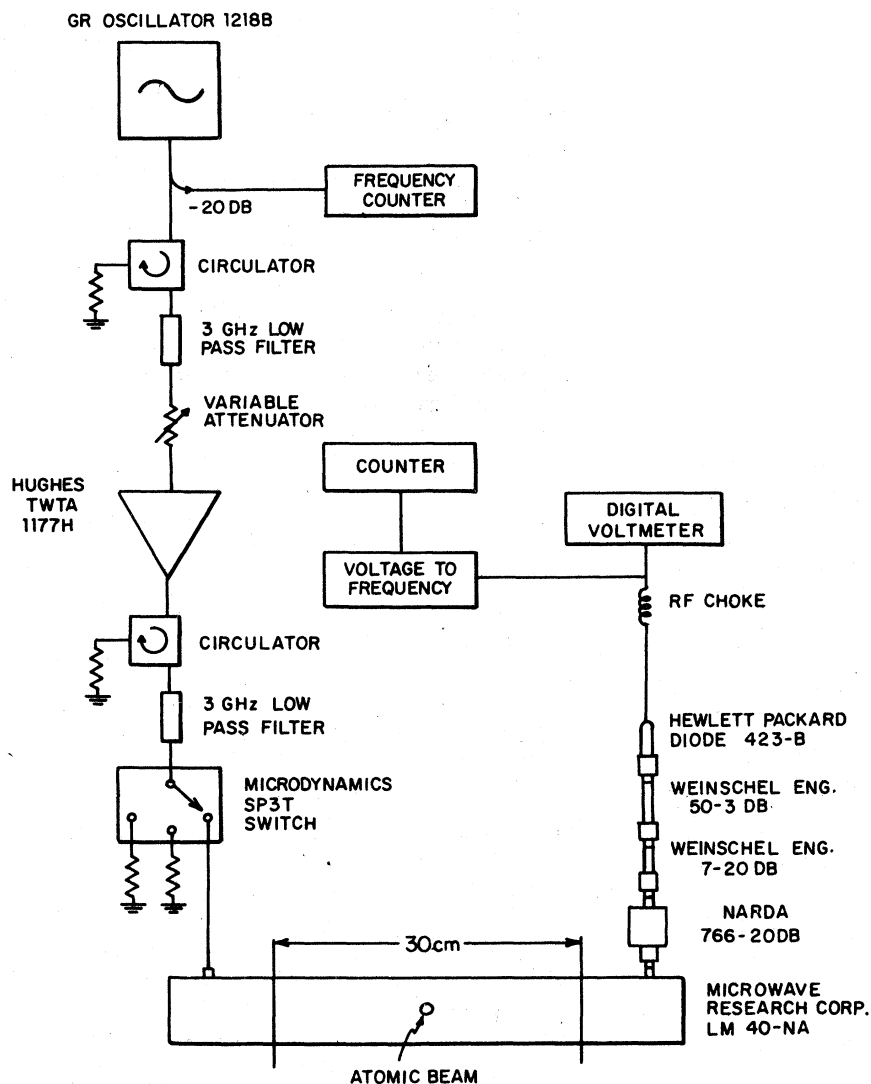
GR OSCILLATOR 1218B

FREQUENCY COUNTER

-20 DB

CIRCULATOR

3 GHz LOW PASS FILTER

VARIABLE ATTENUATOR

HUGHES TWTA 1177H

COUNTER

DIGITAL VOLTMETER

VOLTAGE TO FREQUENCY

RF CHOKE

CIRCULATOR

3 GHz LOW PASS FILTER

HEWLETT PACKARD DIODE 423-B

MICRODYNAMICS SP3T SWITCH

WEINSCHEL ENG. 50-3 DB

WEINSCHEL ENG. 7-20 DB

NARDA 766-20DB

30cm

MICROWAVE RESEARCH CORP. LM 40-NA

ATOMIC BEAM

FIG. 4. Microwave spectroscopy system.

this reflection coefficient was also found to be flat in frequency within ±3°. With this information one can calculate the square of the electric field strength at the position of the atomic beam for a constant power level at the entrance to the 3-dB attenuator. The results are shown in Fig. 5, together with a least-squares-fit line whose slope is found to be $(24 \pm 10) \times 10^{-5}$ MHz^{-1}. This slope includes the effects of standing waves within the waveguide, the variation with frequency of waveguide impedance, and the calibration of the attenuation coefficients of the two 20-dB pads. These two attenuators were directly calibrated with a power meter, and were also compared to three precision 20-dB pads which were factory calibrated by three different manufacturers.

The 3-dB pad and the rf diode were calibrated as a single unit using a Hewlett-Packard 432A power meter. This meter has an absolute accu-

racy of ±3%, but by proper operation the relative power measurement accuracy can be improved to 0.1%. The data reduction procedure is such that the absolute accuracy is of less importance than

ELECTRIC FIELD STRENGTH (arb. units)

1.250

1.240

1.230
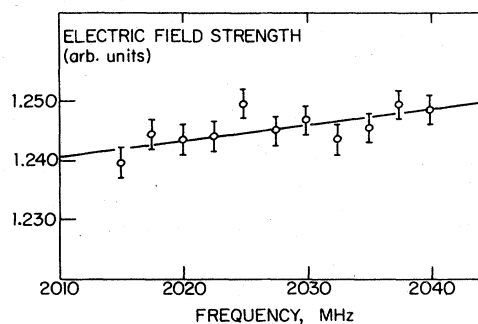
2010   2020   2030   2040

FREQUENCY, MHz

FIG. 5. Square of the electric field strength at the position of the atomic beam for unit power incident on the diode, with best-fit straight line to points.

the relative accuracy, or linearity. That the relative accuracy was 0.1% was ascertained by several consistency checks performed in the laboratory, and accounts for the uncertainty quoted for the diode response versus frequency and for the diode response versus power level.

The attenuators, and rf diode in particular, have a temperature dependence, and so were maintained at a constant temperature with forced air and water cooling, sufficient to dissipate up to 30 W of microwave power. The fractional variation in sensitivity with temperature of the rf diode was measured to be −0.47% per °C, which required that the temperature be maintained constant to ±0.15 °C.

The rf diode output voltage was converted to a frequency and stored in counter A, as well as being read on a digital voltmeter. Although slight drifts in the power level occurred during the taking of a data point, any necessary corrections to the data could be performed afterwards using this counter information. Drifts in the rf diode monitoring circuitry were less than 0.1% of the power level.

The microwave oscillator used to generate the spectroscopy power was unstabilized, but exhibited frequency drift of less than 10 kHz during the taking of a data point.

IV. DATA ACQUISITION

To provide for a thorough test of our understanding of the experimental apparatus and of the lineshape theory, we acquired three complete, independent sets of experimental data for three different atomic beam speeds. These speeds were achieved by using incident H_3^+ ion kinetic energies of 28, 36, and 53 keV, resulting in $H(3S)$ speeds of $10^3 v/c = 4.70$, 5.25, and 6.25, and transit times of atoms through the waveguide of 91.8, 82.3, and 69.0 nsec, respectively. For each velocity, the experimental data can be divided into two broad classes: symmetric points data, which is used to locate the center of the F_0 resonance, and supplementary data, which is used to make corrections to and checks on the symmetric points data.

The symmetric points technique of data acquisition gives a method for rapidly locating the center of a symmetric resonance obtained with a constant level of microwave power. Since the double quantum F_0 resonance is not perfectly symmetric, we must correct the raw data for the calculable asymmetries. By measuring the signal at six points on the steeply sloping sides of the resonance line, one obtains the center location and a measure of the asymmetry. The relative location of these six frequencies is shown in Fig. 6. The points labeled RM and LM (right and left middle) were chosen to be symmetric about the line center and separated by 10 MHz, so that they lay near
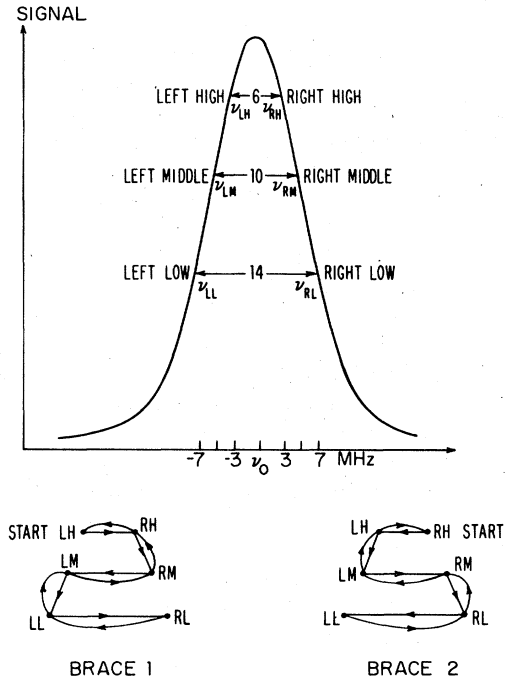

FIG. 6. Arrangement of symmetric points on the two-photon resonance, showing the high, middle, and low symmetric points pairs, and the order in which data were taken.

the half maxima of the curve. The points RH and LH (high), and RL and LL (low), were also chosen to lie symmetrically about the line center, but were separated by 6 and 14 MHz, respectively. The data were taken in at least two sequences of 12 points each as shown in Fig. 6, chosen so as to minimize the effects of drift on the center locations. For each pair of nominally symmetric points, an apparent center for the resonance was deduced. For example, the apparent center found from RM and LM is given by

$$\nu_M = (\nu_{RM} + \nu_{LM})/2 + (S_{RM} - S_{LM})/2m ,$$

where ν_{RM} and ν_{LM} are the frequencies used at the RM and LM points, S_{RM} and S_{LM} are the signals obtained there, and m is the average slope in % per MHz at the RM and LM points (which was found empirically using the points RH, RL, LH, and LL). Similarly ν_H and ν_L denote the centers found from the pairs RH and LH, and RL and LL.

During the acquisition of the symmetric points data for a given experimental configuration and for a given microwave power level, the positions of the six frequencies were modified slightly, maintaining the chosen symmetric points spacings of 6, 10, and 14 MHz, so that the three pairs of symmetric points were kept as symmetric about the center as possible. For each height on the resonance (high, middle, and low) at least four values

for each apparent center (ν_H, ν_M, and ν_L) were obtained. From the scatter in the four or more center values obtained under nominally identical conditions, a standard deviation was obtained. To improve the reliability of this estimate, the standard deviations of ν_H, ν_M, and ν_L were combined in root-mean-square fashion, and the resulting standard error was assigned to all three centers. The errors thus obtained proved to be consistent with those to be expected from purely statistical fluctuations in the number of Balmer α photons counted.

Since the location of the center of the resonance is strongly dependent on the microwave power, it must be measured for many different values of the power. This procedure is motivated by the fact that we can measure the ratio of applied power levels with much less uncertainty than the absolute power at a single point. Since the power shift is primarily linear, we can extrapolate the location of the resonance center to zero power with good accuracy, after correcting the data for the small, calculable higher-order power shifts and other known effects. The power levels chosen for the symmetric points data ranged from 10 W ($E \simeq 14$ V/cm) to 30 W ($E \simeq 24$ V/cm). The high-power limit was fixed by the onset of saturation effects, while the low-power limit was determined by signal-to-noise considerations. Since the signal height scales as the square of the power, it is impractical to measure the line center at very low power. At least seven, and as many as ten, different power levels were used for each atomic beam speed.

Finally, all the symmetric points data had to be acquired for two different configurations of the spectroscopy system. If the atomic beam is not perfectly perpendicular to the spectroscopy waveguide, there will be a first-order Doppler shift of the resonance. This shift may be easily eliminated, however, by acquiring two sets of data, with the direction of microwave propagation reversed between the two sets. This was accomplished by interchanging the microwave source on one end of the waveguide with the attenuators and rf diode on the other, without disturbing the straight section of waveguide through which the beam passes. As this leaves the beam geometry entirely unchanged, the beam's velocity will also be unchanged, so that the first-order Doppler shift of the second set of data is equal and opposite to that of the first. The average result of the two complete sets of data will thus be free of any first-order Doppler shift. In practice, the misalignment was small and the shifts were less than 0.1 MHz.

In summary, for each of three atomic beam

speeds, data were obtained for two microwave geometries, for seven to ten different power levels for each geometry, and for three positions (high, middle, and low) on the resonance for each power level, yielding in all about 200 independent measurements of the resonance center.

The supplementary data were used primarily to make small corrections to the symmetric points data. These data can be subdivided into linescans, state selection data, and saturation data.

Complete panoramic linescans were taken for each beam velocity, for different power levels, and for different conditions of state selection. When the state selection fields were absent, all of the 3S hyperfine states contributed to the observed signal, as shown in Fig. 7(a) for an incident beam energy of 53 keV. The F_1 resonances around 2003 MHz clearly dominate over the desired F_0 resonance near 2028 MHz. Because of the finite transit time of the atoms, these transitions are broadened to about twice their natural linewidth, so the F_1 resonances seriously overlap
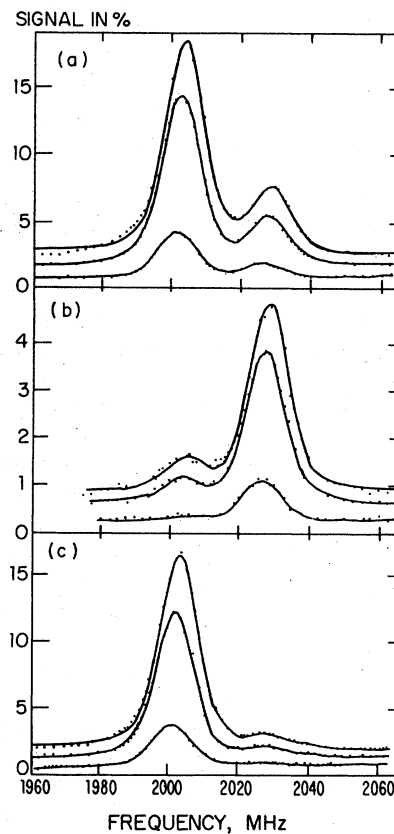

FIG. 7. Panoramic linescans of the two-photon resonances, taken with a 53-keV beam ($T = 69.0$ nsec), and powers of 10, 20, and 30 W: (a) with no state selection; (b) with $F = 0$ states selected; (c) with $F = 1$ states selected.

the desired F_0 resonance. The poor performance of the ion accelerator at lower voltages prevented taking data at still lower beam speeds, so that the natural linewidth was not reached. The solid curves drawn through the data are fits described in the next section.

With state selection fields applied to quench the $3\,^2S_{1/2}(F=1)$ states, the linescans of Fig. 7(b) result. Although the unwanted F_1 resonances are largely suppressed, the residual F_1 components can still affect the center location of the F_0 resonance, so that the symmetric point centers must be corrected for this "hyperfine overlap."

To complete the linescan data, linescans were also taken with the state selection fields applied at 270 MHz to quench the $3\,^2S_{1/2}(F=0)$ states, giving curves as shown in Fig. 7(c). By thus strongly attenuating the F_0 resonance, we can look in detail at the wing of the F_1 resonance in the neighborhood of 2028 MHz, i.e., the location of the F_0 resonance. Except for the relative heights of the F_0 or F_1 resonances, the shapes and locations of these resonances are independent of whether the F_0 or F_1 resonances are quenched. Thus, we may fit the data of Fig. 7(b) to extract the location and width of the F_0 resonance, and substitute this information for F_0 into the fitting of the data of Fig. 7(c). The height of the F_0 component of Fig. 7(c) can then be determined with good accuracy, so that the F_0 resonance can be subtracted from the data. This leaves behind the pure shape of the wing of the F_1 resonance in the neighborhood of 2028 MHz, which can be fit by an empirical function. By normalizing the wing of F_1 to the height of F_1, we can accurately correct the linescans taken with F_1 quenched, such as Fig. 7(b), in the neighborhood of the F_0 resonance.

Since obtaining complete linescans at each power level used in the symmetric points data would have required excessive time, linescans were taken at the lowest-, median-, and highest-power levels used in the symmetric points data, and the information derived from these linescans was interpolated for other power levels. In particular, the shape of the wing of the F_1 resonance near the position of the F_0 resonance was obtained by interpolation. The relative heights of the F_0 and F_1 resonances and the height of the background were directly measured, however, for every power level used in the symmetric points data. These state selection data were obtained by measuring the peak signal at the centers of the F_1 and F_0 resonances, and in the far wings, under the state selection conditions used in the symmetric points data, i.e., with F_1 suppressed. From the known shapes of F_0 and F_1, the relative heights could be obtained from these data, and the contribution of the wing of F_1 in

the F_0 signals could be ascertained.

The correction procedure used in treating the symmetric points data consisted of direct subtraction of the best estimate of the F_1 component from the signals obtained, followed by recalculation of the symmetric points centers mentioned above. The standard errors assigned to the symmetric points centers were suitably (and only slightly) enlarged, to reflect the uncertainty in the size of the F_1 contamination of the F_0 resonance. The size of the corrections entailed by this procedure ranged from 20 to 60 kHz, depending upon the line shape and the efficiency of the state selection system.

The validity of this correction was tested by taking some symmetric points data under conditions of deliberately degraded state selection, in which the heights of the F_0 and F_1 resonances were nearly equal. The symmetric points centers were found to shift by 220 ± 50 kHz from their location under normal state selection conditions. The shift calculated by the correction procedure just described was 200 ± 32 kHz, in good agreement with the observed shift. Since the procedure is observed to work well in these conditions of large shift, we can apply the much smaller actual corrections to the symmetric points data with confidence.

Finally, the symmetric points data were corrected for the slight drifts ($\lesssim 0.5\%$) in the level of microwave power that occurred during the acquisition of a data point. This correction was made by comparing the counts accumulated in the power monitor channel (A, in Fig. 2) with a standard number of counts, and correcting the signal according to the variation in signal size with microwave power observed in the saturation data. In practice, this correction was always quite small compared to the statistical scatter of the signals.

V. DATA REDUCTION AND RESULTS

The reduction of the experimental data falls quite naturally into two separate parts. The first part includes the treatment of the linescans, the saturation curves, and other supplementary data not directly used to locate the center of the resonance. This part of the data provides an excellent testing ground for the theory developed in paper I. The success of the theory in describing details of the experiment gives us confidence in our understanding of the multiple-quantum process. This is most important for the interpretation of the second part of the data, the symmetric points data from which we extract the $3\,^2S_{1/2}-3\,^2D_{5/2}$ energy interval. Many asymmetries and shifts which occur for multiple-quantum resonances cannot be accurately measured experimentally, and so must be

removed from the symmetric points data·with the-
oretical methods.

A. Linescans

The linescans shown in Fig. 7 show the F_0 and F_1
resonances taken under different conditions of state
selection, and different power levels with a transit
time of 69.0 nsec. The solid lines are the least-
squares fit of the line shape calculated to lowest
order (E^4) in TDPT. A background signal which is
allowed to vary linearly with frequency is included
in the fitting program. The two F_1 resonances
are separated by a frequency interval which is
much less than their linewidths, so that it is diffi-
cult to resolve the two components. They are
treated as only one resonance, so that the param-
eters fit to F_1 reveal little about the structure of
the line. All quantities which pertain to the line
shape are derived from the parameters fit to F_0,
which should be well described by the theory.

In our search for an analytical function which
gives a good fit to the resonance line shape, we
tried several empirical functions, such as a Lo-
rentzian, a Gaussian, and the square of a Lo-
rentzian. None of these functions proved to be sat-
isfactory for all beam speeds and power levels.
The function which yields the best fit to the line-
scan data is the lowest-order TDPT line shape de-
rived in the previous paper. While we were able
directly to fit this function to the data, the greatly
increased algebraic complexity of the higher-order
TDPT terms prevented us from including them.
Therefore, our fitting function is unable to account
for power shifts, saturation, or power broadening
of the resonance, all of which are evident in Fig.
7. For this reason, the TDPT line shape works
quite well for the low-power linescans, but works
less well at the highest powers used. Neverthe-
less, its overall performance is considerably
better than the other functions which we tried. The
2×2 effective potential matrix approach, which
should work well at all power levels, was not used
as a fitting function since its calculation by nu-
merical integration is excessively time consuming.

The fitting program using the lowest-order TDPT
line shape returns least-squares-fit values for the
resonance height, center location, and fit transit
time T^*. Figure 8 shows values of T^* returned by
the fitting program as a function of microwave
power; the decrease of T^* with increasing power
is due to the power broadening. This fit transit
time T^* approaches the true transit time T only
when the power approaches zero. The shaded
bands shown in Fig. 8 are the predictions of the
2×2 matrix effective-potential method which in-
cludes power broadening. The line shapes are
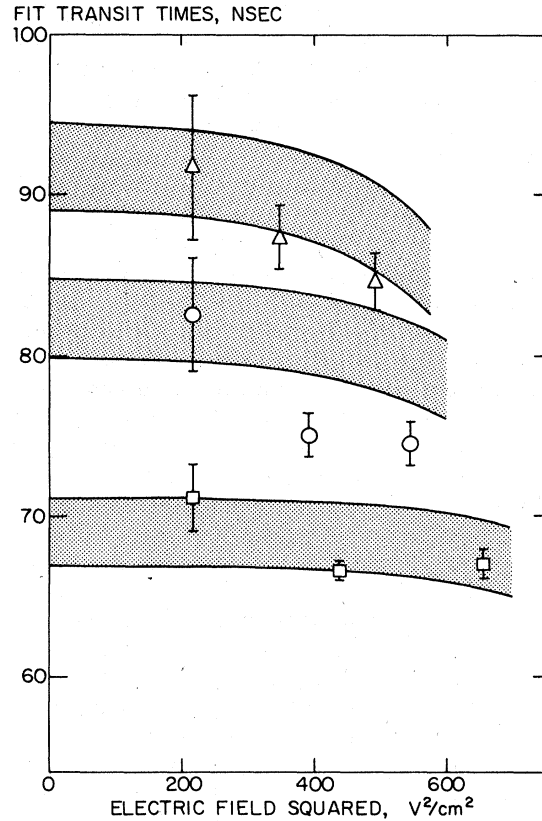calculated a priori using the known beam speed

FIG. 8. Effective transit times T^* deduced from line-
scans of the F_0 resonance. Data points, taken from fits
of the lowest-order TDPT line shape to experimental
linescans; shaded bands, taken from fits of the same
line-shape function to theoretical curves resulting from
the effective-potential matrix approximation (band re-
flecting uncertainty in atomic beam speed).

and microwave power level. The resulting line
shapes are then fit with the TDPT line shape to
produce the fit transit time bands shown. The un-
certainty depicted by these brands arises not from
the theory, but from the 2% uncertainty in the mea-
sured beam speed. The agreement between the fit
transit times from the data and the theoretical
transit times is quite satisfactory.

We note that the observed experimental line-
widths of 10–13 MHz (FWHM) are large compared
to the 5-MHz natural width of the 3S-3D transi-
tion, despite the fact that the experimental transit
times of 70–90 nsec are large compared to the 3D
lifetime of 16 nsec. This apparent paradox arises
from the sinusoidal field distribution in the wave-
guide, together with a transition probability pro-
portional to E^4. A microwave field of constant
amplitude, but of less than half the width of the
waveguide, would produce linewidths comparable
to those we observed.

While the 2×2 effective-potential matrix treat-

ment was not used directly as a fitting function, it is instructive to compare the line shapes which it predicts to the linescan data. Figure 9 shows three linescans taken with a transit time of 69.0 nsec and with 10, 20, and 30 W of microwave power. The solid lines shown are the *a priori* line shapes generated by the matrix approach. The only adjustable parameters are the height of the resonance and the magnitude of the flat background. These adjustable parameters are required by the dilution of the signal with other sources of Balmer α light, as will be discussed below. The atomic energy levels and lifetimes are the theoretical values; the transit time is obtained from the accelerator voltages; the microwave power levels are those directly measured. The 2×2 matrix approximation yields not only the correct power broadening and power shift, but also very close facsimiles of the shape of the observed resonances. We have not subtracted the residuals of the F_1 resonances from these data to emphasize how well the theoretical model and the data agree, without adjustments to either.

In addition to the double-quantum resonance lines, the linescans all contain a background signal, which is nearly constant with frequency. This background signal is primarily the result of nonresonant quenching of the $3\,^2S_{1/2}$ state via an admixture of the $3\,^2P_{1/2}$ and the $3\,^2P_{3/2}$ states, which have much shorter lifetimes. This effect is entirely analogous to the power shift of the $3\,^2S_{1/2}$ state's energy via admixture of the $3\,^2P_{1/2}$ and $3\,^2P_{3/2}$ states, and is easily calculable as the complex part of the $3\,^2S_{1/2}$ state's power shift. Alternatively, one may think of this background as being the far wings of the $3\,^2S_{1/2}$-$3\,^2P_{1/2}$ and the $3\,^2S_{1/2}$-
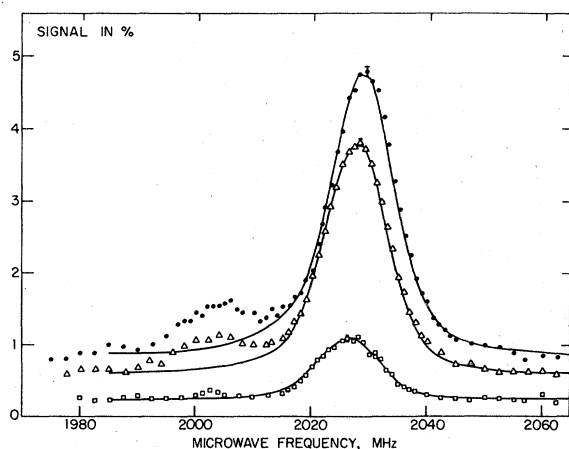

FIG. 9. Linescan data taken with 10, 20, and 30 W of microwave power, and $T = 69.0$ nsec. The solid curves are results of the effective-potential matrix approximation, with only baseline and scale as fit parameters.

$3\,^2P_{3/2}$ resonances. This portion of the background is of little concern since we have an accurate theoretical description of it.

However, the portion of this background signal which originates from atomic states for $n \geq 4$ is a potential source of error for the $3\,^2S_{1/2}$-$3\,^2D_{5/2}$ measurement. A cursory examination of any of the linescan data reveals that the F_0 resonance saturates at a signal height of about 5% or less. The reason for this is the presence of higher-n states formed initially in the gas target cell. States with $n \geq 4$, and those in particular that have large orbital angular momentum, are likely to decay to the ground state with the emission of a Balmer α photon. The most likely decay path for any n state with orbital angular momentum greater than 2 passes through the $3D$ state; this is certain to happen for the states $4F$, $5G$, $6H$, and so on. Since the lifetimes of these excited states are quite long, many of these states will be detected by the photomultiplier tube, and will therefore dilute the desired experimental signal. While it is difficult to calculate the exact amount of cascade light that is expected, a simple analysis explains the observed saturation of the F_0 resonance at a few percent. If we take $1/n^3$ as giving the relative population of the nth Bohr level and assume that the states within any n manifold are equally populated, then the $3\,^2S_{1/2}(F=0)$ substate constitutes 4.0% of the total number of states with $n \geq 3$. This is as consistent with the data as can be expected, given that this calculation ignores the details of the decay process. In addition, residual gas in the vacuum system may emit light under excitation by the incident ion beam.

Simple dilution of the signal by the cascade light does not present any problem other than producing slow drifts in the signal height. Such drifts could result from changes in the pressure in the target cell and elsewhere, which affect the populations of the excited states. If any of these excited states with $n \geq 4$ are affected by the spectroscopy fields, however, the linescans will have structure not predicted by the analysis of the $n = 3$ manifold. The worst possible situation, that of a resonance in a higher-n state occurring near 2025 MHz, may be ruled out by examining the energy-level diagram. There is no single- or multiple-quantum resonance in states with $n \geq 4$ within several hundred MHz. The very strong microwave fields in the spectroscopy region can produce significant, nonresonant quenching in high-n states by the same mechanism described earlier for the $3\,^2S_{1/2}$ state. Since all resonances for $n \geq 4$ are less than 2 GHz in frequency, one might suspect that a slight slope with frequency in the background signal would occur, with the background level from

cascades decreasing as the frequency is increased. To test for this possibility, the linescans were extended far into the wings of the F_1 resonance, and the least-squares fitting program allowed to search for a linear slope with frequency in the background. The results from all of the linescans are consistent with zero slope, with an uncertainty of $\pm(5 \times 10^{-4})\%$ per MHz. Such a slope can produce a shift in the apparent center of the F_0 resonance of 1 kHz at most.

B. Saturation data

Another experimental test of the 2×2 matrix effective-potential theory is provided by analysis of the saturation behavior of the F_0 resonance. This is a particularly stringent test since the higher-order terms in E are approximately handled in the formulation of the effective potential. Data were taken to study the saturation behavior using points at the center of F_0, at the center of F_1, and in the far wing of F_0. A simple inversion of these data using the known resonance line shapes yields the true height of the F_0 resonance above the background signal, as a function of microwave power. This eliminates the need for complete linescans,
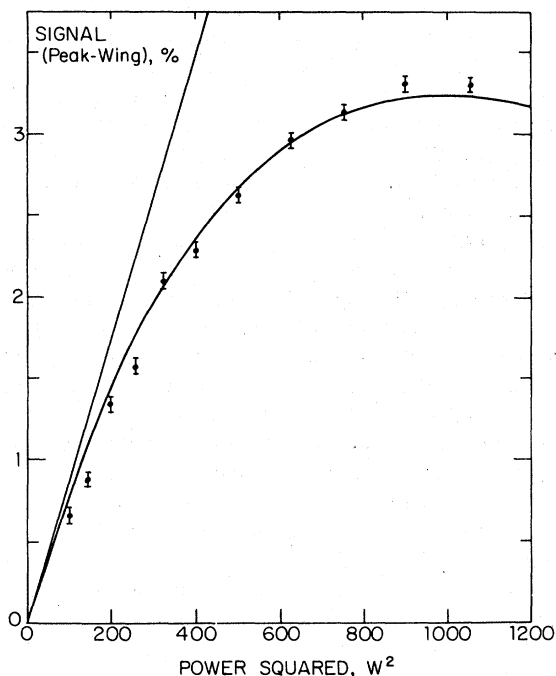

FIG. 10. Saturation data for the F_0 resonance, taken with $T = 69.0$ nsec. The upper theoretical curve is the lowest-order TDPT result; the lower, the effective-potential matrix result. Data and theory formed from difference of signals at peak of resonance and wing at 2060 MHz. A single adjustment is made to the overall vertical scale.

which are subject to long term drifts in signal height. Figure 10 shows the height of F_0 as a function of the power squared, for a transit time of 69.0 nsec. The lowest-order TDPT calculation produces the straight line, which illustrates unsaturated E^4 growth of the signal. The curve is obtained from the 2×2 matrix effective-potential approximation, and represents an *a priori* calculation of the saturation behavior, using the experimental values for the beam speed and microwave power level. There are no adjusted parameters other than a single vertical scale factor, accounting for the signal dilution. While the lowest-order TDPT prediction is in error by a factor of 3 at the highest-power level, the 2×2 matrix effective potential shows very satisfactory agreement with the data.

In summary, the lowest-order TDPT line shape is found to provide the best analytical function for the least-squares fit of the linescan data, particularly at low-power levels. The 2×2 matrix effective-potential method gives an excellent reproduction of the line shape, and accurately predicts the power broadening and saturation behavior of the double-quantum resonance.

C. Symmetric points data

After the hyperfine overlap and power drift corrections have been made, the symmetric-points data can be analyzed using the 2×2 matrix effective-potential theory. All of the symmetric points data were simulated with the 2×2 matrix theory, using the measured beam speed and microwave power level as input parameters. The simulations provide predictions for ν_H, ν_M, and ν_L symmetric-points centers, which are found from symmetric points spaced by 6, 10, and 14 MHz, respectively, on the resonance line shape.

The measured and the predicted centers may differ for several reasons. First and foremost, the input value of 4051.080 MHz used in the simulation for the $3\,^2S_{1/2}(F=0)$-$3\,^2D_{5/2}(F=2)$ interval may not be correct; such an error will give a uniform difference between data and theory. Second, the absolute value of the microwave power level (i.e., the scale) may be incorrect; this will produce differences between the data and simulation which are linear in power. Third, the simulation does not include the first- or second-order Doppler shift. However, the Doppler effects will only shift the centers by a constant amount, and corrections for them are easily made. The $\vec{E}'$ $= \vec{v} \times \vec{B}$ shift discussed in the previous paper is included in the simulation. There are other shifts predicted by the simulation which are neither independent of, nor linearly dependent upon, the

power level. Chief among these is the higher-order power shift, which for points obtained at the highest-power levels amounts to at most an 80-kHz departure from a purely linear power shift. Since, however, the absolute power level is known to ±3%, such corrections introduce negligible uncertainty in the simulation.

In order to isolate the difference between the input and the actual value of the $3\,^2S_{1/2}(F=0)$-$3\,^2D_{5/2}$ $(F=2)$ interval, and any error in the absolute power scale, we form for each subgrouping of the symmetric points data the difference between experimental and simulated centers, and least-squares fit these differences or residuals to a straight line. The intercept of this line at zero power gives the difference between actual and input values for the fine-structure interval, while the slope of the line is a measure of any error in the power scale.

This procedure is illustrated in Fig. 11, where in Fig. 11(a) are shown the experimental values for the ν_M line centers taken with $T=82.3$ nsec and in one Doppler geometry. The solid curve in Fig. 11(a) is the a priori simulation using the known transit time and microwave power levels. The differences, or residuals, are plotted in Fig. 11(b), together with the best-fit straight line. The intercept at zero power is one of 18 such intercepts entering the final answer for the fine-structure interval.

At this point, the first- and second-order Doppler-shift corrections were applied. The first-order Doppler shift for each beam speed is removed by averaging the zero-power intercepts for the two Doppler geometries. Subtraction of the zero-power intercepts for the two geometries yields the first-order Doppler shifts of 0.190 ±0.128, 0.183 ±0.088, and 0.138 ±0.115 MHz for beam speeds of $10^3 v/c = 4.70$, 5.25, and 6.75. From the known beam speeds, the misalignment angle of $(0.6 \pm 0.2)°$ from exact perpendicularity between the waveguide and the beam axis is deduced. This deviation is consistent with what is expected from the alignment procedure for the waveguide. The second-order Doppler shift is calculated from
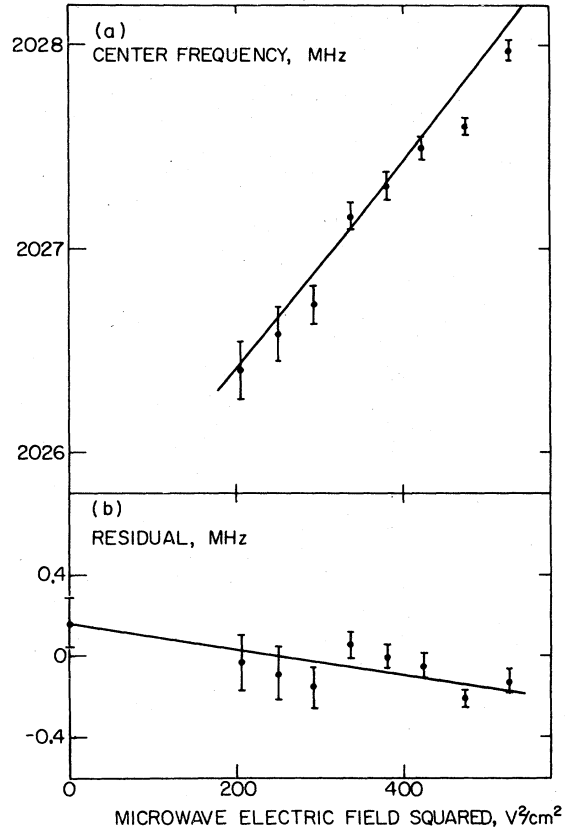

FIG. 11. (a) Observed symmetric points centers, obtained for the M ("middle") symmetric points, in one of the two Doppler configurations, at $T = 82.3$ nsec. Smooth curve is the a priori (not fit) effective-potential matrix approximation prediction. (b) Residuals between data and simulation, fit to a line as described in text. Extrapolation to zero power gives 1 of 18 such line centers.

$$\Delta\nu = \tfrac{1}{2}(v^2/c^2)\nu.$$

For the three beam speeds of $10^3 v/c = 4.70$, 5.25, and 6.75, the corrections are +0.022, +0.028, and +0.040 MHz, respectively, with errors to be discussed later.

This procedure gives the nine independent values for the $3\,^2S_{1/2}(F=0) = 3\,^2D_{5/2}(F=2)$ interval shown in Table I, corresponding to the three beam speeds

TABLE I. Extrapolated line centers, in MHz. Columns give results for different transit times; rows, for different symmetric points spacings. Column, row, and overall averages are also shown.

		Transit time (nsec)			
		91.8	82.3	69.0	Average
Symmetric point	H	2025.902(111)	2025.605(75)	2025.493(100)	2025.641(53)
	M	2025.387(111)	2025.573(75)	2025.524(100)	2025.517(53)
	L	2025.557(11)	2025.541(75)	2025.451(100)	2025.520(53)
	Average	2025.615(64)	2025.573(43)	2025.489(58)	2025.559(30)

TABLE II. Experimental power shifts, MHz cm^2/V^2, deduced from the data in the manner described in the text.

| | | Transit time (nsec) | | |
		91.8	82.3	69.0
Symmetric point	H	4.35(29)	4.61(18)	4.79(20)
	M	5.85(29)	4.90(18)	4.75(20)
	L	5.56(29)	4.76(18)	4.89(20)

and the three determinations of the center, ν_H, ν_M, and ν_L, from the three locations on the resonance line shape. When suitably averaged, these nine values produce the best estimate of the $3\,^2S_{1/2}$-$3\,^2D_{5/2}$ interval.

Before this is done, however, we first examine the symmetric points data for other information which can be used to test the 2 × 2 matrix effective-potential theory. This information can be obtained from two sources, the asymmetry of the resonance and the size of the linear power shift.

To examine the asymmetry of the line shape, we form the differences $\nu_H - \nu_M$, and $\nu_M - \nu_L$ for all of the raw symmetric points centers, i.e., before the residuals are formed. The simulated values for these differences are also computed for each of the data points. The predicted asymmetry of the resonance line shape as expressed by $\nu_H - \nu_M$ and $\nu_M - \nu_L$, varies from −11 to 44 kHz for the most extreme cases. If the experimental values for these asymmetries are averaged, the results are

$$\nu_H - \nu_M = 15 \pm 15 \text{ kHz}, \quad \nu_M - \nu_L = 30 \pm 15 \text{ kHz}.$$

The same averaging of the predicted asymmetry yields

$$\nu_H - \nu_M = -4 \text{ kHz}, \quad \nu_M - \nu_L = 10 \text{ kHz}.$$

The agreement between the observed and simulated line centers further supports the 2 × 2 effective-potential matrix approximation.

The size of the linear power shift may be extracted from the nine least-squares fits of the residuals to straight lines. From these data we deduce the power shifts shown in Table II, where the

errors quoted are purely statistical and do not include the error introduced by the uncertainty in the absolute power level. As in the case of line-shape asymmetry, the corresponding linear power shifts are calculated from the simulations, and the ratios of experimental to theoretical values are formed, as shown in Table III. A weighted average of all nine ratios gives the value 0.967 ± 0.016, where the error quoted is purely statistical. This ratio will differ from unity if the absolute power scale is in error. When we include the estimated 3% error in the absolute power scale, the ratio becomes 0.967 ± 0.034, which is consistent with unity. This represents agreement between observed and *a priori* calculated values of the power shift of the two-photon resonance. Since the scale error in the absolute power level should affect all of the data equally, it is instructive to examine the statistical consistency of the nine ratios which yield the purely statistical result of 0.967 ± 0.016. The χ^2 for these numbers is 16.2 for 8 degrees of freedom. The scatter in these nine ratios is partially attributable to the reproducibility of the power monitoring diode. This variation in the absolute scale is not important for the extrapolation to zero power since that procedure depends only upon the relative, not absolute, measurement of power. The averaged value for these nine ratios, with the error increased by an amount which gives a χ^2 of 8 for 8 degrees of freedom, 0.967 ± 0.023, may be interpreted as calibrating the power meter to an absolute accuracy of 2.3%.

Finally, the nine values for the zero power centers listed in Table I are examined. If one forms the average result of ν_H, ν_M, and ν_L for each of the three beam speeds, one finds the results listed across the bottom of Table I. These seem to show a slight trend with beam speed, but are statistically consistent with $\chi^2 = 2.31$ for 2 degrees of freedom. It is important to note that the consistency would be considerably worsened if the lifetime shift, the second-order Doppler shift, or the $\vec{E}'$ = $\vec{v} \times \vec{B}$ effect had been omitted. Alternatively, if one forms the average values for ν_H, ν_M, and ν_L over the beam speeds, one finds the results listed in the right-hand column of Table I. These values

TABLE III. Ratios of experimental to theoretical power shifts, with weighted averages.

| | | Transit time (nsec) | | | |
		91.8	82.3	69.0	Average
Symmetric point	H	0.872(62)	0.927(41)	0.966(45)	0.922(31)
	M	1.157(62)	0.973(41)	0.952(45)	1.027(31)
	L	1.066(62)	0.930(41)	0.968(45)	0.988(31)
	Average	1.032(36)	0.943(24)	0.962(26)	0.979(24)

TABLE IV. Final corrections and error budget, in MHz.

extrapolated line center	2025.559(30)
hyperfine overlap, sloping background	0.000(12)
first-order Doppler shift cancellation	0.000(2)
second-order Doppler shift uncertainty	0.000(3)
lifetime-shift uncertainty	0.000(13)
quadratic power-shift uncertainty	0.000(10)
microwave power scale nonlinearity	0.000(10)
waveguide impedance and reflections	−0.017(7)
dc Stark and Zeeman shifts	0.000(7)
holes for beam in waveguide walls	0.000(1)
net line center	2025.542(39)
$3\,{}^2S_{1/2}(F=0)-3\,{}^2D_{5/2}(F=2)$ interval	4051.084(78)
$3S$ hyperfine structure	−39.457(1)
$3D$ hyperfine structure	+ 1.577(1)
$3\,{}^2S_{1/2} - 3\,{}^2D_{5/2}$ interval	4013.204(78)

for ν_H, ν_M, and ν_L have a $\chi^2 = 3.56$ for 2 degrees of freedom, which has an 18% occurrence rate. The asymmetry remaining in the zero-power extrapolated centers is $\nu_H - \nu_M = 0.124(75)$ MHz and $\nu_M - \nu_L$ −0.003(75) MHz, which are consistent with zero. This indicates that the asymmetry in the experimental data has been successfully removed by the 2×2 matrix approximation. If one forms a direct average of all nine zero-power centers, one obtains 2025.559(30) MHz. This has a $\chi^2 = 14.1$ for 8 degrees of freedom, which has an 8% occurrence rate. While the size of χ^2 is not comforting, chance fluctuations are not ruled out. One might expand the error bars until χ^2 is reduced to 8.0 for 8 degrees of freedom. This could be accomplished by multiplying all errors by 1.33 and would change the statistical uncertainty from 30 to 40 kHz. The size of χ^2 might suggest that the estimates of the errors, derived from the consistency of line centers obtained over a time period of 1 h, are too small and fail to account for drifts and instabilities which occur over longer time scales. We have elected not to expand the errors, since no actual discrepancy in the data has been found, and will take the weighted average 2025.559(30) MHz as the best estimate of the extrapolated line center.

The systematic corrections and uncertainties remain to be applied to this value. The results are summarized in Table IV. The only nonzero correction is labeled "waveguide microwave characteristics" and corresponds to the shift in the line center introduced by the variation of waveguide impedance and reflection coefficients with frequency, as discussed in Sec. III.

The uncertainty listed under "first-order Doppler shift" represents any imperfect cancellation of first-order Doppler shifts due to nonrepeatability

of beam speed from run to run, while that under "second-order Doppler shift" arises from a generous error assignment to the actual speed of the beam, which was calculated from the measured accelerator voltages. An error of 13 kHz is assigned to the lifetime-shift correction, which represents about $\frac{1}{10}$ of the size of the lifetime shift, and more than covers any uncertainty in the atomic lifetimes and energy defects used to calculate it. We assign a 10-kHz error for quadratic power shift, since reasonable models for quadratic power shifts not already included in the analysis produce changes smaller than this in the extrapolated line center. Any nonlinearity in the microwave power scale can produce an apparent quadratic power shift, and another 10-kHz error, reflecting an upper limit on power meter nonlinearity, has been assigned to cover this. The errors caused by dc Stark and Zeeman shifts, and by the holes in the sides of the waveguides, were discussed in the previous paper, and are estimated to be 7 and 1 kHz, respectively.

The application of these corrections and uncertainties yields the net line center listed in Table IV. Doubling this frequency, and its error, gives the experimental $3\,{}^2S_{1/2}(F=0)-3\,{}^2D_{5/2}(F=2)$ energy separation. There remains only the hyperfine-structure correction to be added to give the more conventional $3\,{}^2S_{1/2}-3\,{}^2D_{5/2}$ interval. The hfs correction, computed in the previous paper, has error of 1 kHz or less.

The final experimental line center of 2025.542(39) MHz has an assigned error of about 20 ppm, arising mostly from statistics. The quoted experimental error of 39 kHz may be compared to linewidths of 10–13 MHz (FWHM), power shifts of 1–3 MHz, lifetime shifts of 100–160 kHz, first-order Doppler shifts of about 150 kHz, and second-order Doppler shifts and $\vec{E}' = \vec{v} \times \vec{B}$ shifts each of 20–40 kHz. In addition there are various smaller shifts and uncertainties.

Despite the somewhat large size of these corrections, we have demonstrated self-consistency among line centers obtained at different beam speeds and different symmetric point spacings. We have found agreement between theoretical and experimental power shifts. We have shown that the mutual consistency of the data is improved by properly including the lifetime shift. Consequently we believe the final answer and its error bars are trustworthy.

VI. CONCLUSIONS

The final result of this paper is the value for the fine-structure interval

$$\nu(3\,{}^2S_{1/2}-3\,{}^2D_{5/2}) = 4013.204(78) \text{ MHz}.$$

This is in agreement with an earlier published result[5] of

$$\nu(3\,^2S_{1/2}\text{-}3\,^2D_{5/2}) = 4013.152(98)\text{ MHz}$$

derived from the same data by a somewhat less sophisticated analysis than that described here. This new result represents an order-of-magnitude improvement in precision over the best previous measurement[6] of

$$\nu(3\,^2S_{1/2}\text{-}3\,^2D_{5/2}) = 4013.800(800)\text{ MHz}.$$

It is also in good agreement with the prediction of quantum electrodynamics[7]

$$\nu(3\,^2S_{1/2}\text{-}3\,^2D_{5/2}) = 4013.197(7)\text{ MHz}.$$

The result of this paper may be combined with the well understood $3D$ and $3P$ fine-structure separations and the small $3\,^2P_{3/2}$-$3\,^2D_{3/2}$ level shift to give an indirect value of the $3S$ Lamb shift of

$$\nu(3\,^2S_{1/2}\text{-}3\,^2P_{1/2}) = 314.887(78)\text{ MHz}.$$

This may be compared to a previous single-quantum measurement[4] of

$$\nu(3\,^2S_{1/2}\text{-}3\,^2P_{1/2}) = 314.819(48)\text{ MHz}$$

and with the QED prediction[7] of

$$\nu(3\,^2S_{1/2}\text{-}3\,^2P_{1/2}) = 314.896(7)\text{ MHz}.$$

The results of this paper mark the first time that a two-photon resonance has been resolved to so small a fraction of its linewidth, or had its power shift so accurately measured. Both a good experimental situation and a careful analysis of the line shape were required to achieve this.

The fundamental limit in precision of this experiment has not yet been attained. Many of the systematic problems can be reduced by using the fast beam separated oscillatory fields techniques.[4,8] These techniques have been demonstrated to work on the $3\,^2S_{1/2}$-$3\,^2D_{5/2}$ transition in exploratory experiments.[9,10] The separated fields experiments should provide a considerable improvement in precision over that reported here, with the result that the most precise value of the $3S$ Lamb shift would come indirectly from a two-photon measurement of the $3S$-$3D$ fine-structure interval.

ACKNOWLEDGMENTS

---

*Present address: Physics Dept., Brandeis University, Waltham, Massachusetts, 02154.

[1]D. A. Van Baak, B. O. Clark, and F. M. Pipkin (preceding paper), Phys. Rev. 19, 787 (1979).

[2]H. Kleinpoppen, Z. Phys. 164, 174 (1961).

[3]L. R. Wilcox and W. E. Lamb, Jr., Phys. Rev. 119, 1915 (1960).

[4]C. W. Fabjan and F. M. Pipkin, Phys. Rev. A 6, 556 (1972).

[5]B. O. Clark, D. A. Van Baak, S. R. Lundeen, and F. M.

Pipkin, Phys. Lett. A 64, 172 (1977).

[6]M. Glass-Maujean, Opt. Commun. 8, 260 (1973).

[7]G. W. Erickson (private communication).

[8]S. R. Lundeen and F. M. Pipkin, Phys. Rev. Lett. 34, 1368 (1975).

[9]P. B. Kramer, S. R. Lundeen, B. O. Clark, and F. M. Pipkin, Phys. Rev. Lett. 32, 635 (1974).

[10]B. O. Clark, D. A. Van Baak, and F. M. Pipkin, Phys. Lett. A 62, 78 (1977).